Period elongation-based framework for operative assessment of the variation of seismic vulnerability of reinforced concrete buildings during aftershock sequences

Konstantinos Trevlopoulos[1*] and Philippe Guéguen[1]

[1] ISTerre, CNRS/IFSTTAR, Université Joseph Fourier, BP 53, 38041 Grenoble CEDEX 9, France

[*] Corresponding author:
k.trevlopoulos@gmail.com

ABSTRACT

Safety assessment of structures and/or critical infrastructures is a key factor in post-seismic decision-making. In this context we present a performance-based framework for modeling time-variant vulnerability of reinforced concrete buildings during aftershock sequences. Structural damage is associated with first eigenperiod elongation, a performance metric whose measurement can complement visual inspection and assessment of structural health as a post-seismic operative tool. The proposed framework is applied for a series of reinforced concrete building models and two aftershock sequences. Damage states are defined using thresholds of period elongation. Numerical models of the buildings in each damage state are considered and their fragility curves are computed. The time-variant vulnerability is modeled with Markov chain as a function of the characteristics of the aftershocks sequence. Finally, the probabilities of the damage states are computed as a function of time during two real aftershock sequences.

Keywords: reinforced concrete, structural degradation, seismic vulnerability, time variation, cascading events, aftershock sequence

Reference:

Trelopoulos K., Guéguen P. 2016. Period elongation-based framework for operative assessment of the variation of seismic vulnerability of reinforced concrete buildings during aftershock sequences, Soil Dynamics and Earthquake Engineering, doi: 10.1016/j.soildyn.2016.02.009

1. INTRODUCTION

Earthquakes are the principal cause of degradation of the properties of structural elements in reinforced concrete (RC) buildings. Stiffness degradation is one of the reasons that modern seismic codes, such as Eurocode 8 [1], demand the stiffness of structural elements to be taken into account with its effective value, which equals a portion of the stiffness of the geometric section of each member. Apart from stiffness degradation, an increase of the damping ratio of the building may accompany seismic damage and affect its response. Another source of structural degradation is the aging effect and the natural deterioration of the structural materials. Pitilakis et al. [2] estimated the detrimental effect of the corrosion of steel reinforcement with time-dependent fragility curves of multistory buildings. Sanchez-Silva et al. [3] proposed a stochastic model that takes into account the effect of gradual non-seismic deterioration of structural materials along with the structural deterioration due to sudden events such as earthquakes and highlighted the importance of both modes of deterioration.

For the case of earthquake clusters such as aftershock sequences, Iervolino et al. [4] developed a probabilistic damage accumulation model for elastic-perfectly plastic single-degree-of-freedom (SDOF) structures and estimated the failure probability as an increasing function of time. Repeated earthquakes and the subsequent damage accumulation may lead to an increase of the inelastic displacement demand of SDOF systems and an increased ratio of the inelastic displacement to the maximum displacement of the elastic system [5]. According to Miranda and Ruiz-Garcia [6], degrading SDOF structures have higher strength and ductility demands than non-degrading structures, when excited by seismic input with a predominant period which is higher than their natural period. Mouyiannou et al. [7] assessed damage accumulation in masonry buildings due to the 2010-2012 Canterbury earthquake sequence and proposed state-dependent fragility curves for masonry buildings with pre-existing damage.

One way of quantifying the structural degradation of a building is through the elongation of its fundamental period. Cracking of reinforced concrete elements due to static loads, in addition to the presence of infill walls, is considered to affect significantly the elongation of the natural period of buildings [8]. Katsanos et al. [9] estimated that period elongation does not exceed 1.2 and 1.7 for the design earthquake and twice the design earthquake, respectively, in the case of moment resisting frames and dual structural system multi-story buildings designed with Eurocode 8. Only in extreme cases of severely degrading buildings a ratio of 2.0 was estimated. Katsanos and Sextos [10] proposed an empirical function for period elongation based on the structural period and the force-reduction factor. Moreover, they showed that Peak Ground Acceleration (PGA) has a low correlation with the

predominant inelastic period in contrast to spectral acceleration. Based on measurements in damaged buildings after the 2011 Lorca earthquake Vidal et al. [11] proposed relationships for the period of the damaged buildings as a function of the number of stories. According to these relationships the period elongation is independent of the number of stories and equals 20 %, 43 % and 65 % for EMS [12] damage grades 1, 2 and 3-4. These results are approximately equal to observations by Dunand et al. [13] for equivalent damage levels, who were certainly the first who associated the classical in-situ red-orange-green traffic light classification of damaged buildings with period elongation after the 2003 Boumerdes, Algeria earthquake. The period elongation ratio has been observed to be proportional to the stiffness and the force-reduction factor (ratio of the maximum seismic force to yield force) of SDOF oscillators [9], while the effect of earthquake magnitude, distance and soil conditions has been estimated to be of minor significance.

Jeon et al. [14] have developed aftershock fragility curves for reinforced concrete buildings in California. These aftershock fragility curves give the probability to exceed damage thresholds given the intensity measure and an existing damage state caused by the mainshock. Their most interesting finding is that buildings with damage caused by the mainshock, which is less or equal to moderate, have less than 4 % additional probability to develop severe damage in the aftershock sequence. Ebrahimian et al. [15] developed a performance-based framework in order to make operative forecasts for the first day after the mainshock. They computed event-dependent fragility curves and estimated the daily risk of exceeding of damage thresholds using synthetic aftershock sequences, which were generated with the Epidemic Type Aftershock Sequence model. Yeo and Cornell [16] introduced Aftershock Probabilistic Hazard Analysis and assessed the vulnerability of a building in a series of damage states in order to assess the time-variant probability of collapse. They also employed Markov chain analysis to estimate financial losses due to structural damage. The probability of collapse and financial loses constitute the input of their decision tree analysis framework for earthquake risk management.

The variation of the vulnerability immediately after the mainshock is a key factor in post-seismic decision-making. Given that reinforced concrete buildings may accumulate damage during aftershock sequences and become more vulnerable, it is necessary to employ procedures, which estimate the variation of seismic vulnerability during aftershock time-periods. The presentation of such a procedure is the aim of this article. This article, in contrast to previous work on this topic, focuses mainly on an efficient operative method proposed for assessing time-variant vulnerability during aftershock sequences. This method is based on the assessment of resonance frequency shift, which can be related to damage states ([11], [13]) and the associated variation of fragility curves. Period elongation assessment can be used complementary and in support of visual inspection of buildings and

expert judgment after a damaging earthquake. Furthermore, the proposed framework could be used to update vulnerability functions in an early-warning protocol (e.g. [17]). The building models considered herein are representative of critical infrastructures such as the Port of Thessaloniki, which is the site of one of the case studies. The structural health of such buildings is often monitored with proper instrumentation. Since structural degradation can be observed and localized through eigenfrequency variation ([18], [19], [20]), we have defined damage-state thresholds in terms of the relative increase of the period, as measured before an earthquake in the undamaged building and afterwards in the damaged building. The reduced stiffness of the structural elements of the degraded building models and period elongation is expressed as a function of total and maximum inter-story drift computed by non-linear time-history analyses. Once the relationships between maximum inter-story drift and period elongation have been estimated, the thresholds of the damage states are defined using period elongation values and the fragility curves of the original and degraded models are computed. The fragility curves are subsequently used to compute state transition probabilities in the Markov chain used to model the time-variation of vulnerability. The probabilities of the considered damage states are finally computed in the cases of two real aftershock sequences as application examples of the proposed framework, a detailed risk analysis with the proposed framework or a sensitivity analysis of its results are out of the scope of this article.

2. BUILDING MODELS

A series of low-rise and mid-rise reinforced concrete building models (Fig. 1) is selected as representative of typological categories in Greece [21]. The models are being referred to as C1L, C1M, etc. using the naming convention in HAZUS [22] according to building type. The characteristics of the selected models are summarized in Table 1 and include low-code and low-rise models of buildings with a structural system of bare (C1L) and regularly infilled (C3L) moment resisting frames, shear walls equivalent system (C2L) of frames coupled with shear walls carrying more than 65 % of the base seismic shear force [23]; a mid-rise C1M type building models with low, moderate and high seismic code design; and a mid-rise low-code C2M building model. The rationale behind including bare frame in the analyses is that although the presence of infill walls is generally regarded as beneficial for the structure, when their layout is regular [21], it has been shown that their presence may be detrimental and their modeling can be challenging [24]. As far as the period of the C1M high-code building model is concerned (Table 1), it is higher than the periods of the C1M low- and moderate-code building models because of smaller dimensions of the seismic load-bearing structural members contrary to what would be expected. Low-code design level refers to seismic

design according to the first seismic code that came into effect in Greece in 1959, while moderate design level is according to 1985's Supplementary Clauses and high-code level corresponds to design with the Greek seismic code of 2001 [25]. The provisions of the 2001 code bear similarities to EN 1998-1 [23] and demand capacity design with structural member detailing for ductile behavior aiming for energy dissipation in the seismic resisting system and plastic building collapse mechanisms. According to a 2001 survey, 32 % of the building stock of Greece predated the 1959 code, 46 % was constructed between 1959 and 1985, when a new seismic code was introduced, under which 22 % of the stock was built [26]. Based on more recent data in the city of Grevena in Greece, the reinforced concrete buildings built after 1959, 1985 and 2001 consist 49 %, 11 %, and 19 % of the building stock, respectively [27].

Three types of analyses are performed with OpenSees [28]: fiber, modal and non-linear time-history analyses. All building models are two-dimensional and p-delta effects are not included in the analyses. Although simplified 2D models are unable to account for effects related to irregularities such as torsion, it has been shown that they can be used to make an effective estimation of losses of real 3D structures [21]. The fiber analyses are employed to compute the yield moment and curvature of each structural element through a bilinear approximation of the numerical results. This data is then used in non-linear analyses to model the inelastic response of the elements with a distributed plasticity model of hysteretic response with stiffness degradation. Pinching in the moment-curvature loops is used only for the structural walls with a factor of 0.3 assuming a strong pinching effect. The infill walls are modeled with double diagonal struts with a compressive strength of 3.2 MPa and an elastic modulus of 3.2 GPa. Modal analyses are used to compute the fundamental period of the models in their undamaged and damaged states. In the total mass of each model, which is assumed to remain constant as the building deteriorates, the mass corresponding to structural elements, infill walls, live and dead loads of the slab floors are included. According to the code for interventions in existing buildings in Greece [29] in inelastic analyses the bending stiffness (EI) of structural elements should be taken into account equal the secant stiffness at yield, which is averagely 25 % or less of the stiffness (EI_g) of the geometric un-cracked section [23]. Since a hysteretic law with stiffness degradation is used for bending behavior in the dynamic analyses, which models stiffness degradation after yield, the stiffness of the elements is taken into account equal to a fraction of the un-cracked stiffness, which fits the moment-curvature results of the fiber analysis. In all time-history analyses Rayleigh damping is used with a 5 % ratio and the effect of structural degradation on the damping of the structure is ignored in the absence of relevant guidelines.

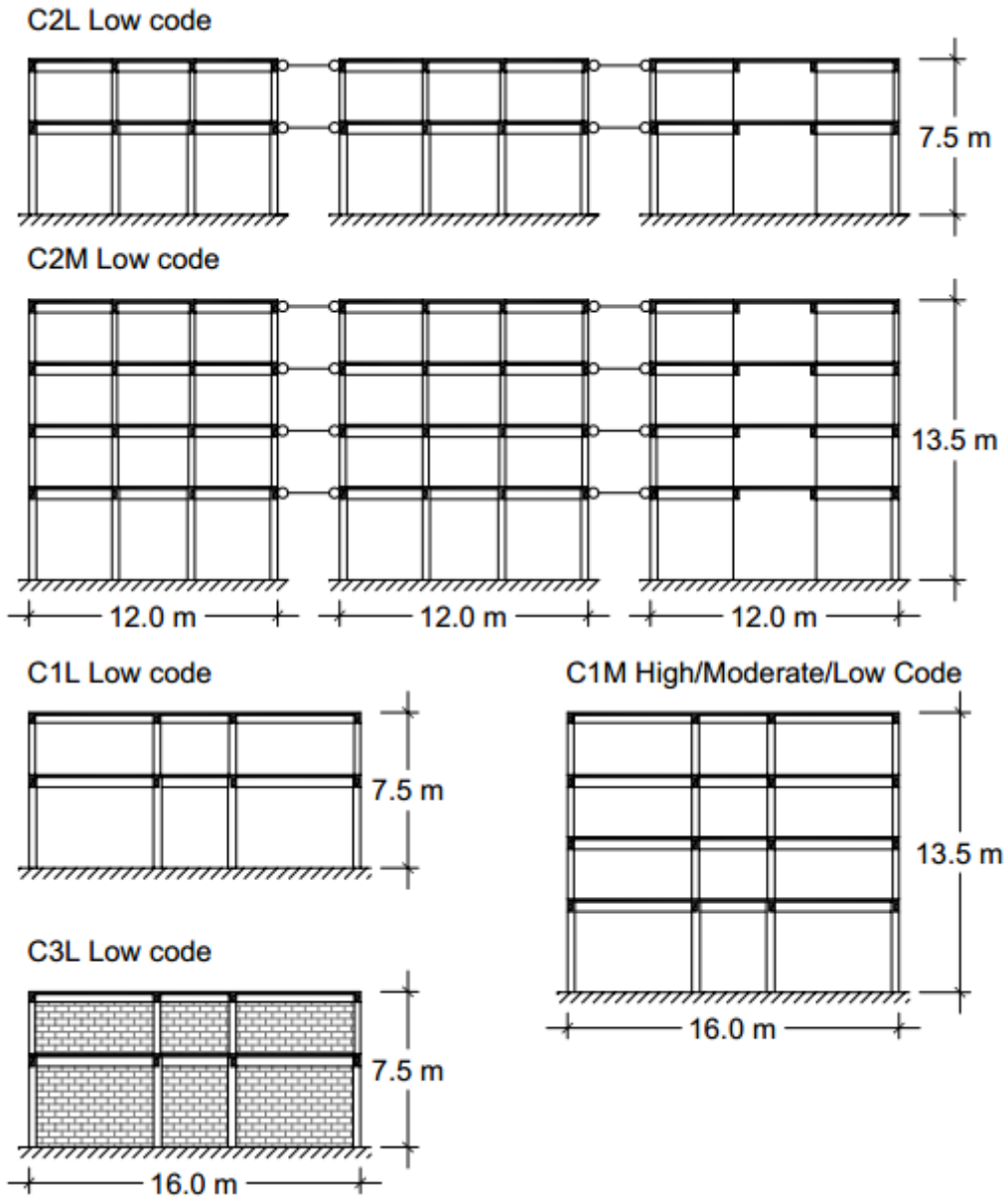

Fig. 1 Configuration of the studied building models representing reinforced concrete buildings in Greece

Table 1 Details of the studied building models

Building Type	Structural System	Height (number of stories)	Seismic Design Level	$T_{1,orig.}$ (s)
C1L	Moment resisting frames	Low-rise (2)	Low code	0.48
C2L	Shear walls equivalent			0.18
C3L	Regularly infilled frames			0.20
C1M	Moment resisting frames	Mid-rise (4)		0.61
C1M			Moderate code	0.62
C1M			High code	0.64
C2M	Shear walls equivalent		Low code	0.38

3. FRAMEWORK DESCRIPTION

The variation of the vulnerability of the studied buildings during an aftershock sequence is modeled probabilistically through seven steps, which include the group of interconnected actions shown in Fig. 2:

1. Inelastic time-history analyses of the undamaged building model prior to the main shock are performed in the context of Probabilistic Seismic Demand Analysis with excitations leading to structural response, which ranges ideally from elastic to extensively inelastic.

2. The stiffness degradation of element sections is estimated as a function of total drift and the degraded stiffness of the structural elements in the drift range of interest (e.g. 10^{-4} - $6 \cdot 10^{-2}$) is computed. A series of modal analyses is performed, each corresponding to the state of the building at each drift value considered. In each modal analysis the degraded stiffness of element sections is computed with the estimated functions leading to the estimation of the first eigenperiod of the equivalent linear model of the degraded building ($T_{1,deg.}$) and leading to period elongation as a function of drift. This step is analyzed further in section 4.

3. The damage state thresholds are defined in terms of elongation of the first eigenperiod of the original building model ($T_{1,orig.}$) due to structural degradation and corresponding story drift. The degraded building models are formed by computing the stiffness of element sections at the defined period elongation thresholds and are then analyzed with the same set of excitations used to analyze the initial state model.

4. The fragility curves of the building models in selected damage states (DS = j, j = 1-m) are computed. The intensity measures (IM) for which the fragility curves are computed in this study are the PGA,

5. For each seismic event (Magnitude-distance pair) in the sequence (i = 1-n) the corresponding intensity measure (a_i), e.g. PGA, is computed with a suitable Ground Motion Prediction Equation (GMPE) based on [30] or [31] for Europe. Most of the results of the presented application of the framework are based on the use of PGA as intensity measure rather than spectral response values, as it is considered more convenient for seismic crisis management.

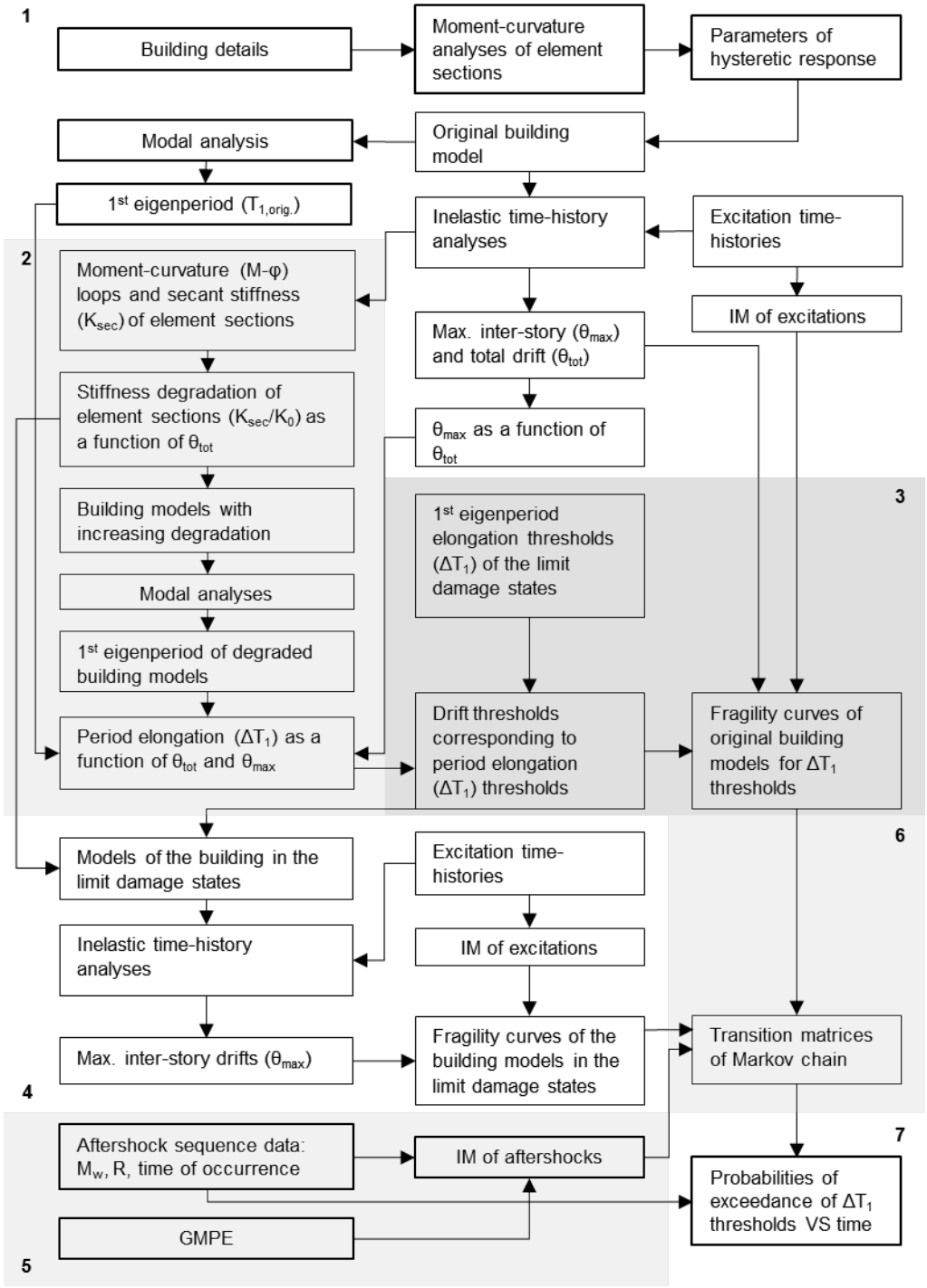

Fig. 2 Flowchart of the proposed framework modeling time-variant seismic vulnerability with consequent steps numbered in bold and described in the text

6. The probability of exceedance of each threshold for the intensity measure values that correspond to the events in the catalog (catalog to be defined) is computed with the fragility curves of the building models in the considered damaged states (numbered 1 to m). The probabilities of exceedance are then used to compute the elements of Markov chain transition matrices according to Chioccarelli and Iervolino [32] considering mutually exclusive and totally exhaustive states [33]. The Markov chain is used to model time-variant vulnerability considering that a building during an aftershock sequence is a system going through a chain of events or states, in which every following state depends only on the current state. Equation 1 gives the general form of the transition matrices ($T_{(ti)}$):

$$T_{(ti)} = \begin{bmatrix} P_{11(ti)} & P_{12(ti)} & \dots & P_{1m(ti)} \\ 0 & P_{22(ti)} & \dots & P_{2m(ti)} \\ \dots & \dots & \dots & \dots \\ 0 & 0 & \dots & 1 \end{bmatrix} \quad (1)$$

The first index denotes the original state and the second index the state to which the systems transitions. Firstly, the elements of the last column are computed with Equation 2:

$$P_{jm\,(ti)} = P\left[DS_{(ti)} = m \mid DS_{(ti-1)} = j, IM_{(ti)} = a_i\right] \quad (2)$$

Equation 2 gives the probability of exceeding the threshold of the highest considered damage state (DS = m) at the time of a seismic event (t_i), given that the building is in a lower damage state (DS = j, j < m) at the previous time-step (t_{i-1}). This value is equal to the value of the fragility curve (of the building model in damage state j) for damage state m, which corresponds to the value of the intensity measure (a_i). P_{jm} is equal to the probability of transition from damage state j to damage state m for the given a_i intensity measure. Subsequently, the elements of each matrix between the diagonal and the last column are computed with Equation 3:

$$P_{jk\,(ti)} = P\left[DS_{(ti)} = k \mid DS_{(ti-1)} = j, IM_{(ti)} = a_i\right] - P\left[DS_{(ti)} = k+1 \mid DS_{(ti-1)} = j, IM_{(ti)} = a_i\right] \quad (3)$$

Equation 3 gives the probability of transition from damage state j to damage state k, i.e. the probability to exceed the threshold of damage state k but not the threshold of state k+1, given that the building is in damage state j (j < k). Both terms of the right hand side of Equation 3 are the fragilities, which result for the value of the intensity measure (a_i). The first and the second term of Equation 3 are equal to the value of the fragility curves (of the building model in damage state j) for damage states k and k+1, respectively. Finally, the diagonal elements are computed with Equation 4:

$$P_{jj\,(ti)} = 1 - P\left[DS_{(ti)} = j + 1 \mid DS_{(ti-1)} = j, IM_{(ti)} = a_i\right] \tag{4}$$

The diagonal elements (P_{jj}) are equal to the probability to remain in damage state j and not exceed the threshold of damage state j+1 for an intensity measure equal to a_i and given that the building is in state j. Similarly to Equation 3, the second term of the right hand side of Equation 4 is a fragility. Elements below the diagonal are assumed to be equal to zero excluding the event of transitioning to a lower damage state and a decrease of structural period after stiffness degradation has taken place. Therefore the Markov chain is irreducible and does not have a stationary distribution. One transition matrix is computed for each seismic event in the sequence as a function of the intensity measure (a_i) and one series of matrices is computed for each building model. Given that the values of the elements of the transition matrix are time-dependent, as they depend on the value of the intensity measure for each seismic event, the Markov chain is time inhomogeneous.

7. The probability of the building being in a damage state at the time points of the aftershocks is computed with a discrete time Markov chain with a discrete time space using the computed transition matrices as follows:

$$[\,P[DS_{tn} = 1]\ \ldots\ P[DS_{tn} = m]\,] = [1\ \ 0 \ldots\ 0] \prod_{1}^{n} T_{(ti)} \tag{5}$$

Zero values have been assigned to all the elements of the starting vector in the right hand side of Equation 5 with the exception of the first element of the vector, which is equal to 1.0. By this it is assumed that the building before the first seismic event of the sequence is in its first state, which here is considered its original undamaged state. With Equation 5 it is also possible to compute the probabilities of being in the defined damage states in the case that

the building is in a higher damage state before any event in the sequence of seismic events by assigning the 1.0 value to the corresponding element of the vector.

4. PERIOD ELONGATION-BASED FRAGILITY CURVES

Damage states are defined based on threshold values of the elongation of the first eigenperiod of the building (ΔT_1). The selected thresholds correspond to the elongation of the period of buildings after the 2011 Lorca earthquake, which sustained damage with a grade of 1 to 4 in the EMS scale [11]. The advantage of using ΔT_1 thresholds is that, since the elongation of the first eigenperiod of a building can be measured by means of instrumentation immediately after the main shock, condition-based damage assessment can be available remotely and in real time without the need for inspection. These damage states are defined using the results of the same set of non-linear analyses used for the computation of the fragility curves of the building in its original state.

4.1. Seismic input time-histories

The time-history analyses are performed to assess the performance of the structure assuming fixed conditions at its base, where the seismic excitation is applied. The probabilistic model, which is used for the seismic demand, is formulated with the ground motion bin approach [34]. Fourteen bins of time-histories are used as input in the time-history analyses and each bin includes 15 synthetic acceleration time histories. A different magnitude-distance combination corresponds to each bin and the used combinations are shown in Fig. 3b.The time-histories of each bin were generated using as average target spectrum the mean acceleration response spectrum, which results from the GMPE of Ambraseys et al. [35] for the bin's magnitude-distance combination. The selected GMPE has been used in [2] to define reference spectra in the context of fragility analysis of reinforced concrete buildings in Greece. By using synthetic accelerograms it is taken into account that the frequency content of the accelerograms corresponds to the selected magnitude and distance. The synthetic time-histories were generated with SeismoArtif [36], which implements a method based on [37]. The PGA of each of the 14 target spectra ranges from 0.5 m/s^2 to 14.3 m/s^2, however individual time histories have a wider range exceeding 20.0 m/s^2 (Fig. 3a). The time-histories of the last three bins have extremely high PGAs, as they have been generated for M_S equal to 7.1, 7.4 and 7.6. Such magnitudes are unlikely to happen given the hazard of Thessaloniki. The time-histories for these magnitudes serve the purpose of estimating structural stiffness degradation in a range that includes extensive inelastic response. Furthermore, the structural response of SDOFs with a period lower than 0.50 s to time-histories with frequency content resulting from scaling in Incremental Dynamic

Analysis [38] may be lower than the response to natural and synthetic records, while being unbiased for SDOFs with a period higher than 0.70 s; the assessment of this bias may be more complex for structures with multiple degrees of freedom [39]. Therefore, we consider the selected synthetic time-histories suitable in the case of the studied low-rise building models, which have a fundamental period lower than 0.50 s.

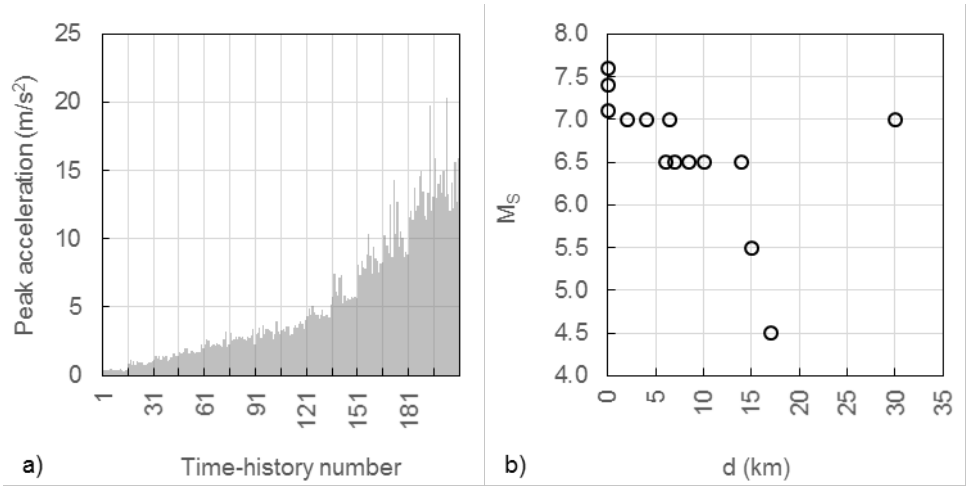

Fig. 3 a) PGAs of the suite of synthetic input motions generated for this study b) magnitude-distance pairs of each bin of input motions

4.2. Structural degradation and period elongation

The stiffness degradation ratio of structural elements is computed as a function of the total drift. The stiffness degradation ratio is defined as the ratio of the secant modulus (K_{sec}) of the moment-curvature loops (Fig. 4), which result at sections along the length of structural elements, to the elastic stiffness (K_0 = EI) of the sections. The elastic stiffness of the sections is computed by taking into account the moment of inertia as the fraction of the moment of inertia of the geometrical section, which fits moment-curvature results of fiber analysis. Reinforced concrete members suffer stiffness reduction due to a series of effects irrelevant to seismic loads such as shrinkage and static loads. Therefore, the period of an undamaged building, which is computed based on pre-seismic measurements is the result of reduced stiffness of reinforced concrete structural members in comparison to their geometric stiffness. Fig. 4 shows the numerical results of the stiffness degradation ratio at the section of the foot of an outer column on the ground floor of the C1M low-code model and at the section of the edge of the adjoining beam. According to the numerical results in Fig. 4c the stiffness of the column degrades at a faster rate, which indicates a probable yield of the column before the beam. Power functions are computed at sections of the beam-column finite elements of the models (excluding data of K_{sec} equal to 1.0) to estimate the variation of stiffness degradation

between the ends of beams and columns and their middle sections. The location of the sections along the length of the elements is defined by the Gauss-Legendre quadrature rule.

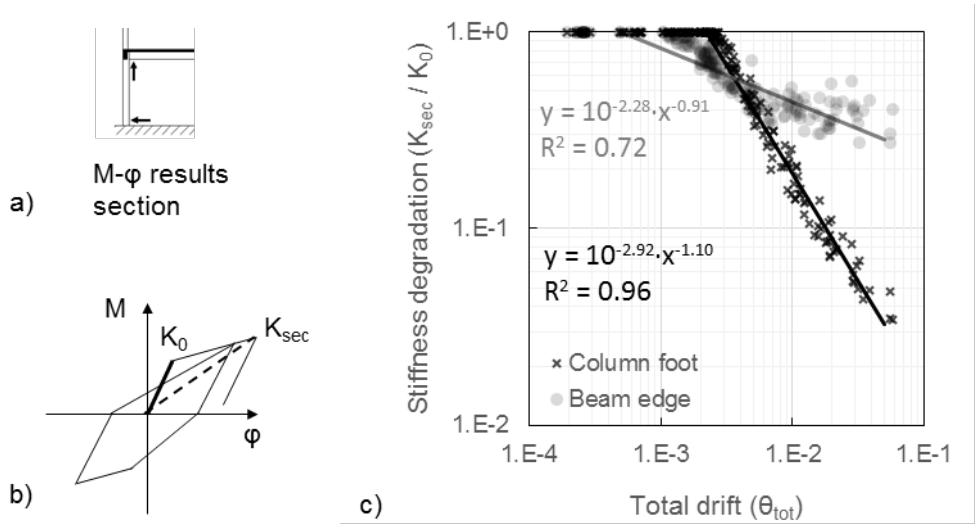

Fig. 4 a) Sections at the foot of an outer column and at the edge of the adjoining beam of the C1M low-code model b) Secant modulus (K_{sec}) computation based on the moment-curvature hysteretic loops resulting at element sections for each input motion c) The ratio of the secant to the elastic modulus (K_0) as a function of the total drift (θ_{total}) according to the results of the inelastic analyses

Prismatic beam elements are used to model the degraded buildings, due to the fact that stiffness degradation varies along the length of each element (e.g. at the top and at the foot of a column more degradation is expected than at middle). The cross-section dimensions remain constant from section to section of each element, however the bending stiffness varies. The mean degraded stiffness at the sections of the finite elements is computed with the analytical relationships, which were estimated based on the moment-curvature results. The uncertainty associated with the estimated degraded stiffness is not taken into account. The computed degraded stiffness corresponds to building response ranging from elastic to extensively inelastic (i.e. total drift of 10^{-4} - $6 \cdot 10^{-2}$). The degraded stiffness is then used in a series of models with increasingly degraded stiffness in order to estimate their fundamental period ($T_{1,deg.}$). In this study the increase of the first eigenperiod (ΔT_1) of the degraded building relatively to the period of the original building ($T_{1.orig.}$) is used as measure of period elongation, given by Equation 6:

$$\Delta T_1 = \frac{T_{1,deg.} - T_{1,orig.}}{T_{1,orig.}} \quad (6)$$

The ΔT_1 as a function of total drift, which results from the modal analyses, is shown in Fig. 5a. Period elongation is observed for all building models for a total drift higher than $1 \cdot 10^{-3}$. Beyond this threshold, period elongation is higher for low-rise models than the mid-rise models. The first eigenperiod elongation of the C2L model begins at a total drift of $6 \cdot 10^{-4}$, which is the lowest observed threshold of period elongation, while the C2M model has the lowest rate of increase of period elongation.

Fig. 5b shows ΔT_1 as a function of the maximum inter-story drift (θ_{max}). The curves in Fig. 5b result from the curves in Fig. 5a by computing the corresponding maximum drift using analytical relationships for the maximum inter-story drift as a function of total drift (θ_{tot}). Such functions were estimated for each building model. Fig. 6 shows the fit of analytical functions to the numerical results of maximum versus total drift in the case of the C1M and C2M low-code models. Table 2 lists the parameters of the fitted functions for all studied models and the coefficient of determination (R^2) in each case. Moment-resisting frame models C1L and C1M have a higher analogy of maximum inter-story drift to total drift than the shear wall models C2L and C2M of equal height.

In this study three damage states are considered and defined using thresholds of ΔT_1 equal to 20 %, 40 % and 60 %. These thresholds cover the range of period elongation that has been observed in reinforced concrete buildings with seismic damage up to Grade 3-4 [11]. The maximum inter-story and total drifts that correspond to the ΔT_1 thresholds are obtained from Fig. 5b and are listed in Table 3. Using the total drifts in Table 3 and the analytical relationships for the stiffness degradation of the element sections, the stiffness of the element sections is computed for each damage state. Buildings in the damage states are then modeled using the values of the degraded stiffness of the element sections, which have been computed for ΔT_1 equal to 20 %, 40 % and 60 %.

Fig. 7 shows the ratio of the degraded stiffness of the prismatic structural elements of the models for the C1M low-code building in damage state for ΔT_1 equal to 20% and 40%. It is noted that short-period structures (< 0.50 s) may demonstrate higher period elongation than long-period structures and equal force reduction factor [10]. Therefore, the same amount of period elongation may correspond to different damage levels for different structures. In order to correspond period elongation to a damage level it would be first required to assess the maximum inter-story drift threshold for that level and then to obtain the period elongation from the curve of period elongation as a function of the drift. Moreover, building-specific thresholds for the maximum inter-story drift would be required (e.g. by means of IDA or pushover analysis). HAZUS sets the collapse threshold at a maximum inter-story drift of 0.0500 and 0.0333 for C2L and C2M buildings, respectively, while Kappos [40] at 0.02 for reinforced concrete buildings in Greece, which demonstrates that generic

thresholds may not be suitable. However, the correspondence of ΔT_1 with damage levels is out of the scope of this study.

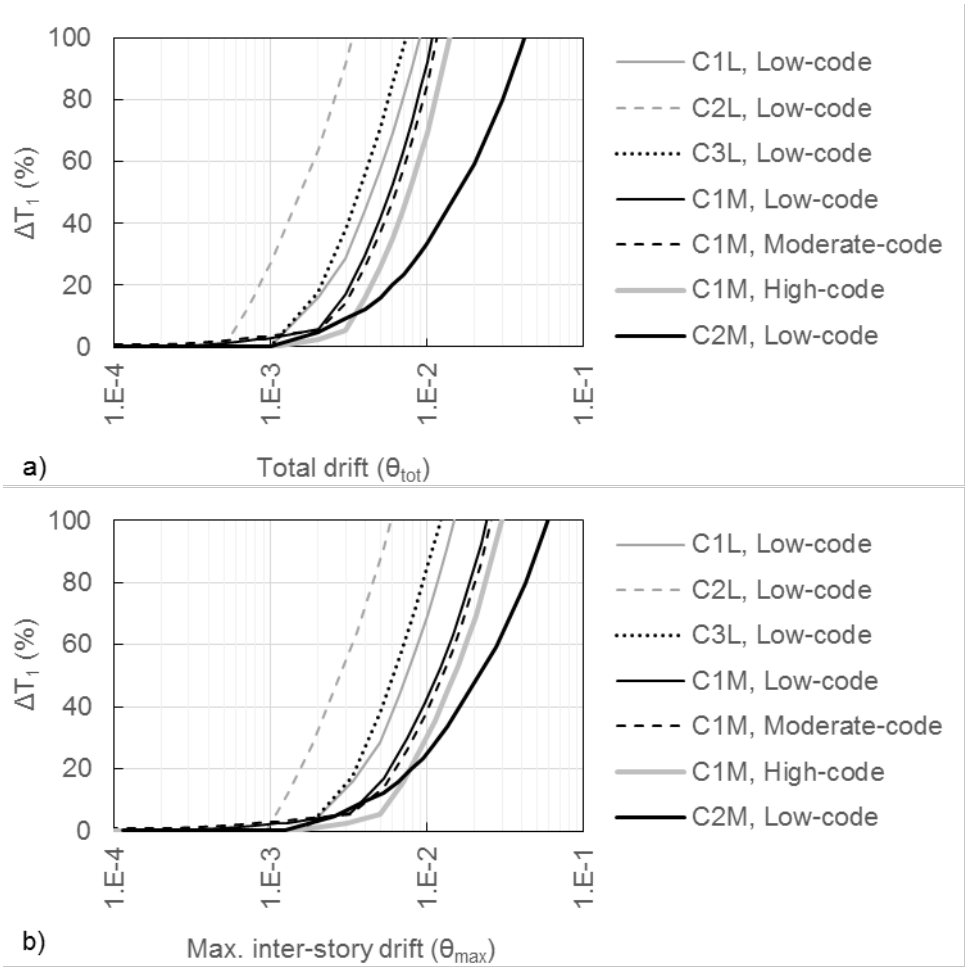

Fig. 5 Period elongation (ΔT_1) of the studied building models as a function of (a) total and (b) maximum inter-story drift

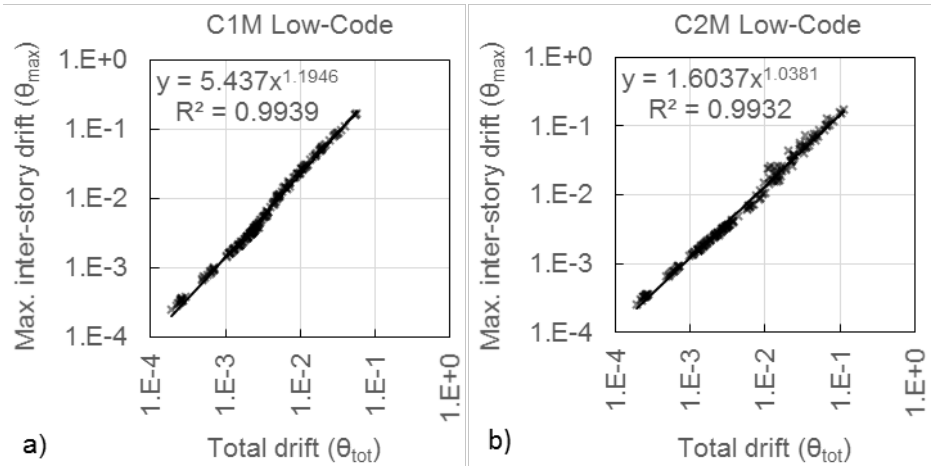

Fig. 6 Maximum inter-story drift as a function of total drift in the case of the (a) C1M and (b) C2M low code building models

Table 2 Maximum inter-story drift as a power function of total drift ($\theta_{max} = a \cdot \theta_{tot}^{b}$)

Building model	a	b	R^2
C1L Low code	1.67	1.00	1.00
C2L Low code	1.49	0.97	1.00
C3L Low code	1.66	1.00	1.00
C1M Low code	5.44	1.19	0.99
C1M Moderate code	5.03	1.18	0.99
C1M High code	4.50	1.17	0.99
C2M Low code	1.60	1.04	0.99

Table 3 Period elongation thresholds and the corresponding maximum inter-story drift (θ_{max}) and total drift (θ_{tot}) for the building models

	θ_{max}			θ_{tot}		
ΔT_1	20 %	40 %	60 %	20 %	40 %	60 %
C1L Low code	0.0041	0.0062	0.0086	0.0024	0.0037	0.0051
C2L Low code	0.0013	0.0020	0.0030	0.0007	0.0011	0.0016
C3L Low code	0.0035	0.0051	0.0071	0.0021	0.0031	0.0042
C1M Low code	0.0058	0.0094	0.0137	0.0032	0.0049	0.0067
C1M Moderate code	0.0063	0.0102	0.0149	0.0035	0.0053	0.0073
C1M High code	0.0078	0.0123	0.0175	0.0044	0.0065	0.0088
C2M Low code	0.0079	0.0170	0.0281	0.0060	0.0125	0.0203

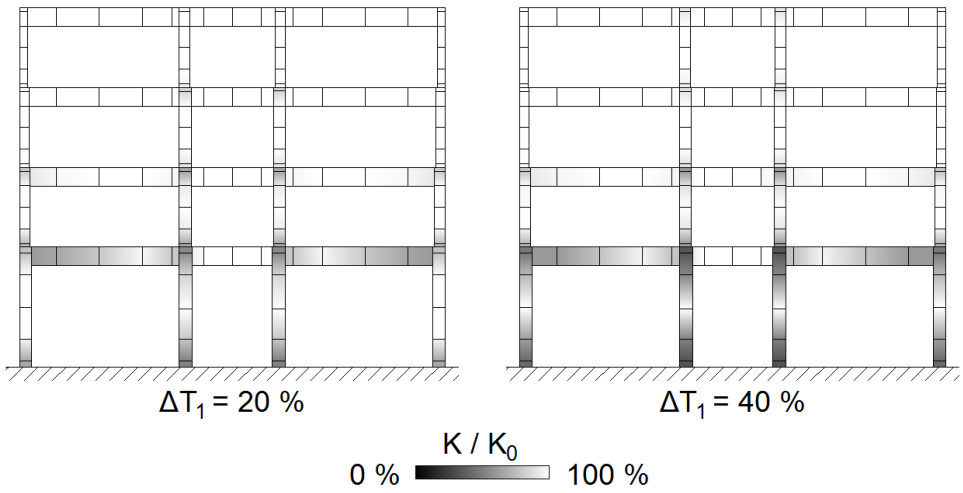

Fig. 7 Ratio of the stiffness of the prismatic structural elements with varying section properties to the stiffness of the corresponding elements in the initial C1M low-code building model (K/K_0) for ΔT_1 equal to 20 % and 40 %

4.3. Period elongation-based fragility curves and state-transition charts

Inelastic time history analyses of the models of the studied buildings in the defined period-elongation-based damage states are used in order to assess probabilistically seismic demands and to compute the fragility curves of the models. The employed set of excitations is the same with the suite of ground motions used in the analyses of the undamaged building models. In Fig. 8 the fragility curves, which have been computed for the building models of this study and for PGA as the intensity measure, give the probability of exceeding a period elongation (ΔT_1) of 20 %, 40 % and 60 % given that the building is in its original undamaged state.

The uncertainties in the computation of the fragility curves are taken into account with the lognormal standard deviation (β), which is constituted by three statistically independent components: the lognormal standard deviations of the definition of the damage states, structural capacity and seismic demand. The lognormal standard deviation of limit state definition is assumed equal to 0.4. The lognormal standard deviation of structural capacity is assumed equal to 0.25 and 0.30 in the case of high- and low-code building models, respectively [22]. In the case of the medium-code building models it is assumed to be equal to 0.28. The total lognormal standard deviation which results (as the sum of squares of its three components) for the studied original and degraded building models is listed in Table 4. A reduction of the total lognormal standard deviation is observed with increasing ΔT_1 for all building models and is more pronounced in the case of the C2L and C2M buildings.

Table 4 Lognormal standard deviation of the fragility curves (as a function of PGA) of the building models in their original (ΔT = 0 %) and degraded states

Building Type	Seismic Design Level	β		
		ΔT_1 = 0 %	ΔT_1 = 20 %	ΔT_1 = 40 %
C1L	Low code	0.63	0.61	0.60
C2L		0.75	0.65	0.61
C3L		0.69	0.62	0.58
C1M		0.61	0.58	0.57
C1M	Moderate code	0.59	0.56	0.54
C1M	High code	0.61	0.59	0.58
C2M	Low code	0.68	0.61	0.60

The maximum inter-story drift that corresponds to the ΔT_1 threshold of 60 % in the case of the C1L bare frame model and the C3L regularly infilled frame model is equal to $8.6 \cdot 10^{-3}$ and $7.1 \cdot 10^{-3}$, respectively (Table 3). Therefore, it is considered that the damage state with the ΔT_1 threshold of 60 % corresponds to a comparable level of damage for the two models, and that the difference of their fragility curves (Fig. 8c) reflects the effect of infill walls. Likewise, the fragility curves of C1M low- and moderate-code models for ΔT_1 = 60 % are considered to

correspond to a comparable degree of damage. The fragility curves of the C1M low- and moderate-code models have no significant differences, which is anticipated given that these models are similar in terms of stiffness and strength and have practically equal period elongation curves (Fig. 5). The fragility curve for ΔT_1 = 60 % of the C1M high-code model has higher values than the curves of the moderate- and low-code C1M models. We consider that this reflects the philosophy of modern-code design for inelastic response. Finally, we observe in Fig. 8 that the fragility curves of the C2M model have lower values than the curves of the C1M models for any of the three considered ΔT_1 thresholds, possibly due to the stiffness and strength of the shear wall, which is included in the model.

Three additional intensity measures are considered herein: pseudo-acceleration (PSA), spectral displacement (S_d) for the first eigenperiod and mean spectral displacement ($S_{d,m}$) between the first eigenperiod (T_1) of the original building and the period which is 30 % higher than T_1. IMs, which are functions of T_1, may lead to lower uncertainties [41]. $S_{d,m}$ is used to take into account transient period elongation, as it has the potential to lead to reduced seismic demand uncertainty ([42]). Accurate estimations of transient period elongation require time-frequency transform of the response. Here 30 % of transient period elongation is adopted as a typical value. Fig. 9 shows fragility curves of the original building models for PSA, S_d and $S_{d,m}$ as the intensity measure. In Fig. 9b-c the fragility curves with S_d and $S_{d,m}$ as IM for the low-rise models (C1L, C2L, C3L) differ significantly from the fragility curves of the rest building models, which are mid-rise. This is attributed to the difference between the median of the fragility curves (Table 5). Such a difference is not observed in the PGA-based fragility curves (Fig. 8) and more IM versus EDP relationships should be studied in further studies. Table 6 shows the log standard deviation of the computed fragility curves of the building models in their original state for the considered IMs. The log standard deviation of the fragility curves for PSA and S_d are equal, as anticipated, as these IMs are equivalent as far as efficiency is concerned [43]. The log standard deviation of the building models with the lowest eigenperiods (C2L, C3L) are significantly higher than the rest and raises the question of IM reliability as a function of building type and building period, in particular for strong level of shaking.

Fig. 10 features six “state-transition charts”, which give the probability of exceeding ΔT_1 thresholds given that the building models are in a lower damage state; e.g. Fig. 10b gives the probability of exceeding ΔT_1 = 60 % given that the building model is in a degraded state with a period elongation of 0 %, 20 % or 40 %. The three curves in Fig. 10b are fragility curves (for the probability of exceeding ΔT_1 = 60 %) of three different building models: the original undamaged C1L low-code model (ΔT_1 = 0 %) and the models of the same building with stiffness degradation corresponding to period elongation of 20 % and 40 %. All state transition charts in Fig. 10 result likewise. State transition charts are computed for all

buildings and all period elongation thresholds in this study. The index t_i is used to denote the time of a seismic event in an aftershock sequence, and t_{i-1} denotes the time of the previous event. The fragility curves in the state transition charts are used to obtain the probabilities in the right hand side of Equations 2-4, which compute elements of the transition matrices of the Markov chain as a function of the IMs of the seismic events. We observe in Fig. 10a-f that the probability of exceeding the period elongation thresholds is higher when the building is in a degraded state (ΔT_1 = 20% or 40 %) than when the building is in its undamaged state (ΔT_1 = 0 %). This observation agrees with the fact that seismic vulnerability increases with structural degradation.

Table 5 Median of the fragility curves of the original building models for exceeding ΔT_1 = 60 % as a function of the IMs in this study

Building Type	Seismic Design Level	$\theta_{\Delta T1 = 60\%}$ PGA (m/s^2)	PSA (m/s^2)	S_d (m)	$S_{d,m}$ (m)
C1L	Low code	2.7	5.8	0.033	0.047
C2L		3.2	7.4	0.006	0.012
C3L		7.4	17.9	0.018	0.034
C1M		6.4	15.2	0.145	0.184
C1M	Mod. code	6.9	16.9	0.162	0.205
C1M	High code	4.2	8.5	0.088	0.110
C2M	Low Code	9.5	24.1	0.085	0.137

Table 6 Log standard deviation of the fragility curves of the building models in their original (ΔT = 0 %) as a function of the considered IMs

Building Type	Seismic Design Level	β PGA	PSA	S_d	$S_{d,m}$
C1L	Low code	0.64	0.65	0.65	0.64
C2L		0.75	0.78	0.78	0.78
C3L		0.69	0.71	0.71	0.71
C1M		0.61	0.62	0.62	0.63
C1M	Mod. code	0.59	0.60	0.60	0.61
C1M	High code	0.61	0.60	0.60	0.60
C2M	Low Code	0.68	0.70	0.70	0.70

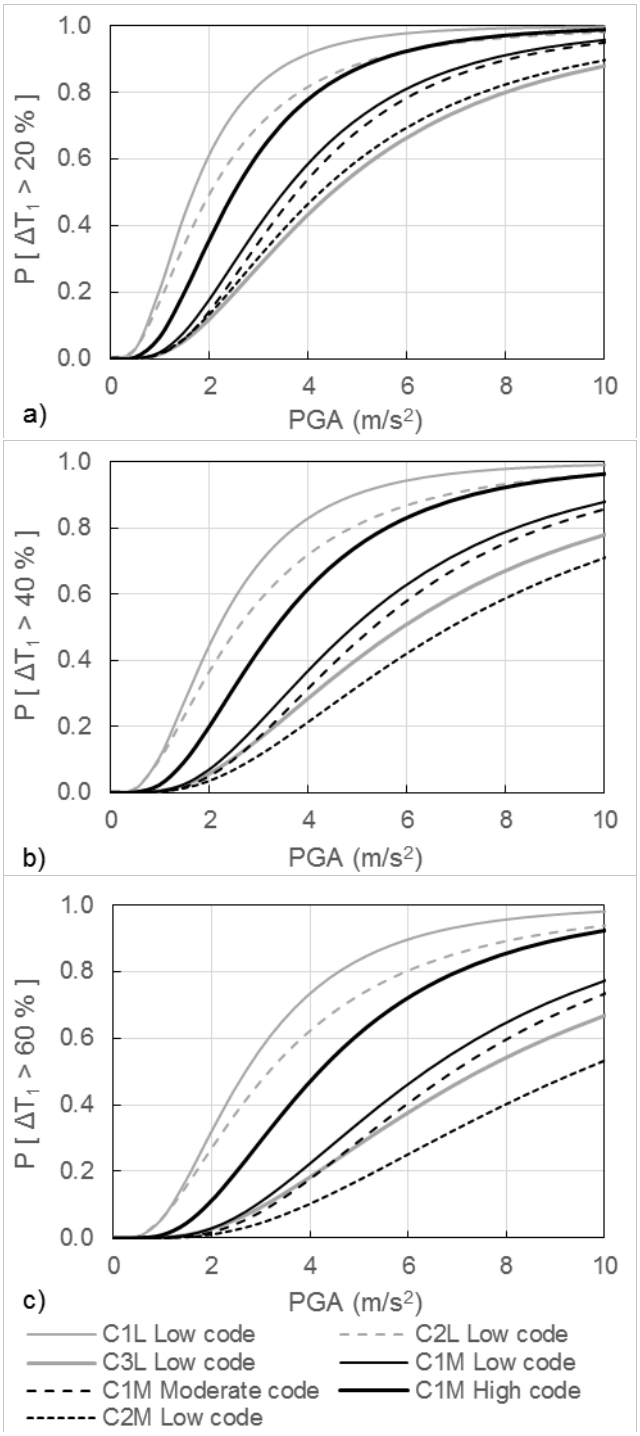

Fig. 8 Fragility curves of the building models for first eigenperiod elongation thresholds of (a) 20 % (b) 40 % and (c) 60 %

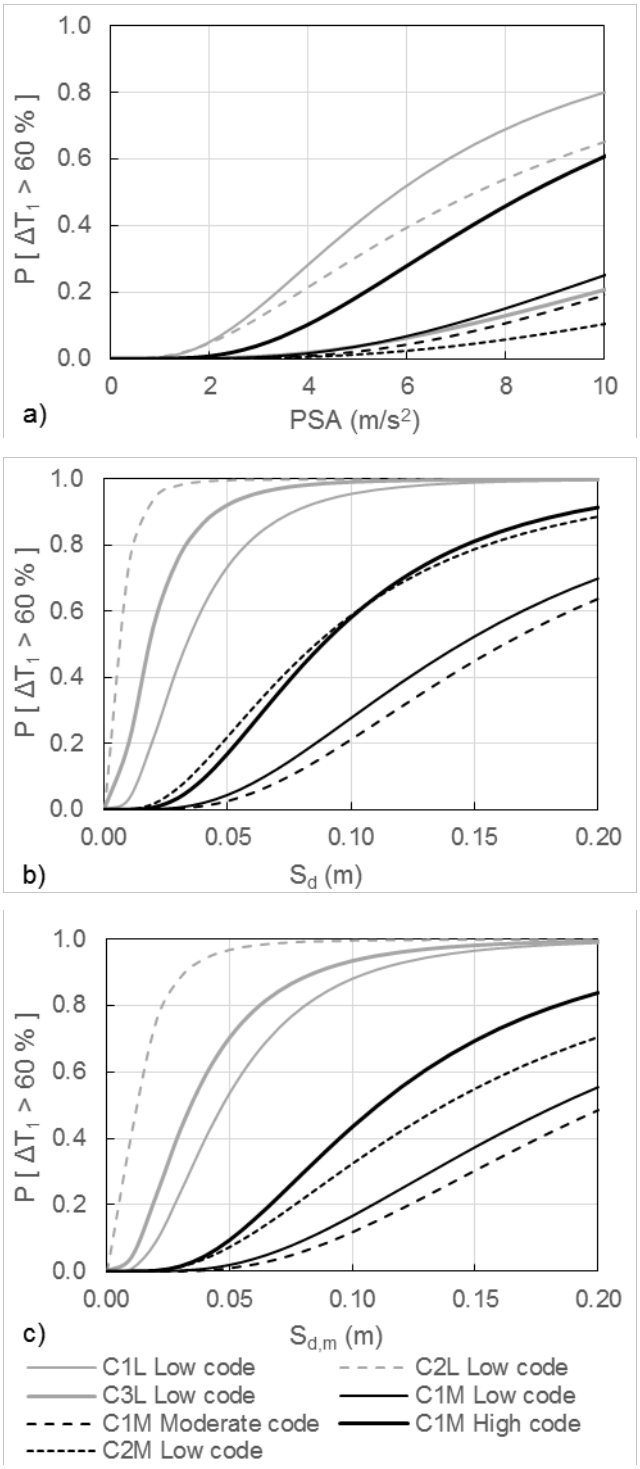

Fig. 9 Fragility curves of the building models for first eigenperiod elongation (ΔT_1) of 60 % for (a) PSA (b) S_d and (c) $S_{d,m}$ as the intensity measure

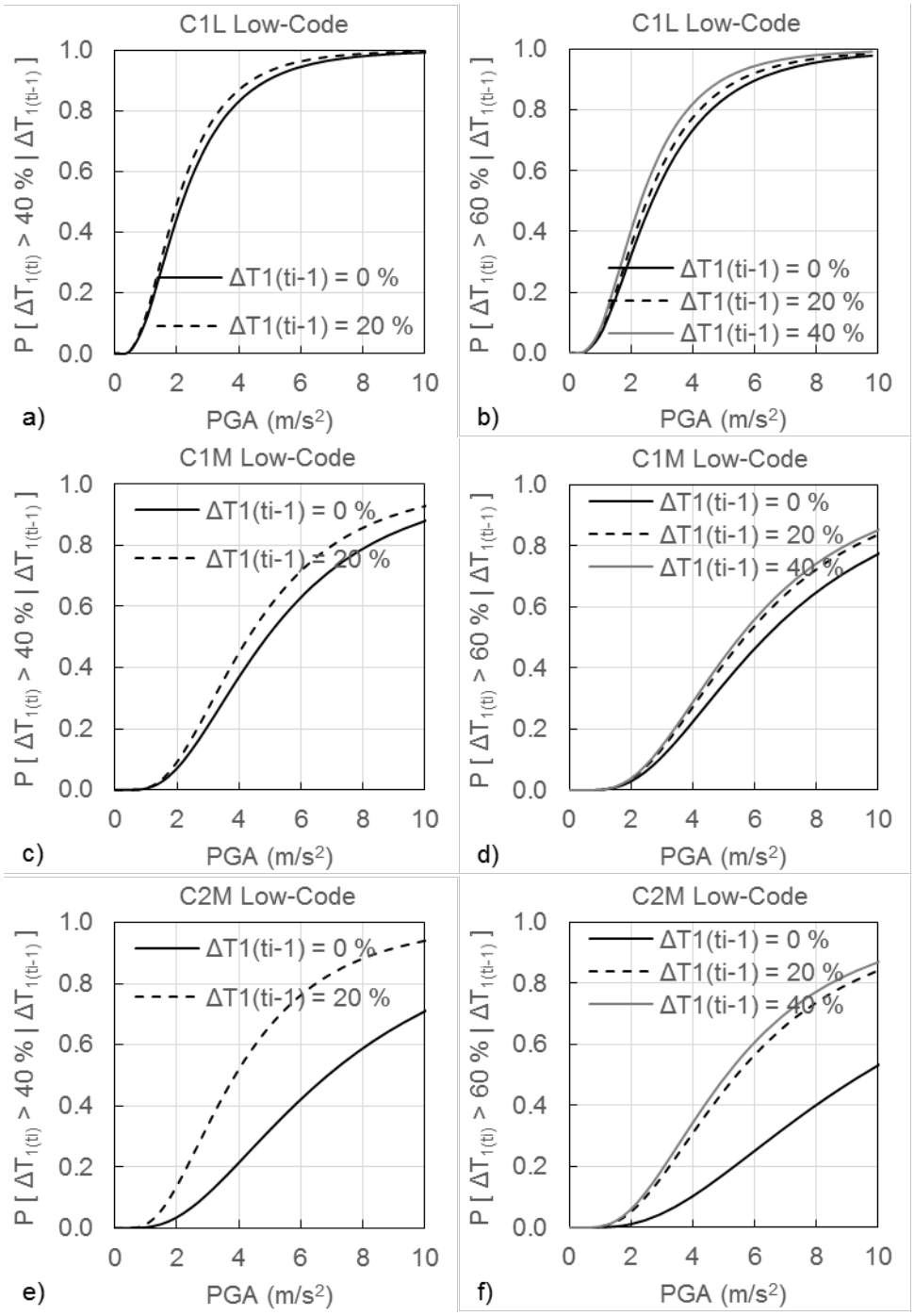

Fig. 10 Probability of transition of the (a) C1L (b) C1M and (c) C2M low-code building models from a period-elongation-based damage state at the previous time point ($\Delta T_{1(ti-1)}$) to a higher damage state at a given time point ($\Delta T_{1(ti)}$)

5. TIME-VARIATION OF VULNERABILITY IN AFTERSHOCK SEQUENCES

The probability of exceedance of the three defined thresholds of period elongation are computed for two cases of real aftershock sequences; the 1978 Thessaloniki (events with M ≥ 4.3 [44]) and the 1994 Northridge aftershock sequence ([45], [46]). The Northridge sequence is employed because of its strong main shock and high number of aftershocks. These two sequences are used to end the framework of the process shown in Fig. 2. For the 1978 Thessaloniki sequence the building location was selected assuming that the building is part of the critical infrastructure of the port of the city without the intention of a specific analysis, while for the Northridge case a hypothetical building location in the State of California is used. The selected building locations have epicentral distances from the 1978 Thessaloniki and 1994 Northridge main shocks equal to 28.2 km and 16.0 km, respectively. In the case of the Thessaloniki sequence the listed magnitudes in the seismicity catalog ([47], [48]) were not adjusted according to Roumelioti et al. [49], but were considered practically equal to the moment magnitude according to Papazachos et al. [50] for simplicity. The PGA at the base of the building for each seismic event is the mean PGA predicted by the GMPE of Akkar and Bommer [51], as it is considered suitable for the tectonic setting of Thessaloniki [31]. The same equation is also used in the case of the Northridge sequence for consistency. The prediction of ground motion parameters such as the PGA is characterized by significant uncertainty and an elaborate approach is recommended for detailed studies including other GMPEs (e.g. [52]) and different types of excitation time series as in [53]. We limit this study to the selected GMPE for simplicity, since our aim is the presentation of the proposed framework.

Fig. 11 shows the moment magnitude (M_w)-epicentral distance (R) pairs of the two sequences and the estimated PGAs during the aftershock periods resulting from the selected building locations. The main differences of the two sequences are the intensity of the shaking, the number of aftershocks and the occurrence time of the main shock in the sequence. Given that the 1978 Thessaloniki main shock (M_w 6.5) has a distance of 28.2 km from the assumed building location, the corresponding PGA is estimated at 0.8 m/s^2, which is lower than 1.5 m/s^2 and 0.9 m/s^2 estimated for the 1994 Northridge main shock (M_w 6.7) and the largest aftershock (M_w 5.3) occurring on the 62nd day of the sequence. The number of seismic events is 63 and 25 in the case of the Northridge and Thessaloniki sequence, respectively. The main shock in the Northridge case is the first event in the sequence, while in the case of Thessaloniki sequence it occurs on the 43th day. Therefore, the Northridge case is a case study of the cumulative probability of exceeding damage levels starting from a state with no structural degradation, and the case of the Thessaloniki sequence is considered as a case study of buildings with accumulated damage before and after the main

shock. In addition, the Northridge sequence is anticipated to lead to higher probabilities of damage not only because of the more intense level of shaking due to the main shock, but also because of the larger number of aftershocks.

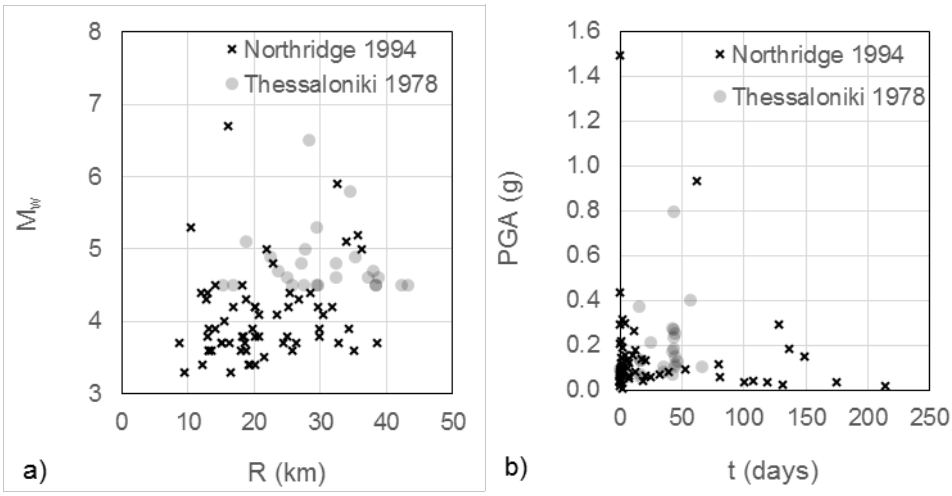

Fig. 11 (a) Moment magnitude-distance pairs and (b) estimated PGAs during the aftershock sequences

The elements of the state transition matrices (Eq. 1) are computed from the values of the fragility curves for PGA produced by earthquakes in the sequence and used in the Markov chain (Eq. 5) to compute the probabilities of the damage states at the time of the seismic events. Equation 7 shows the matrix, which is computed using PGA as the intensity measure in the case of the C1M Low-code model for the 1994 Northridge mainshock. Fig. 12 and Fig. 13 show the results of this computation for the studied buildings for the 1994 Northridge and the 1978 Thessaloniki aftershock sequences, respectively. They also include the probability of the building models to remain in a state with period elongation less than the lowest threshold (ΔT_1 < 20 %). The largest increases of the probability to exceed ΔT_1 = 60 % correspond to the main shock. In the case of the C2M model it amounts to 84 % and 82 % of the total probability to exceed ΔT_1 = 60 % during the 1994 Northridge and 1978 Thessaloniki sequences, respectively.

$$T_{t=0} = \begin{bmatrix} 0.919 & 0.056 & 0.017 & 0.009 \\ 0.000 & 0.966 & 0.023 & 0.011 \\ 0.000 & 0.000 & 0.988 & 0.012 \\ 0.000 & 0.000 & 0.000 & 1.000 \end{bmatrix} \quad (7)$$

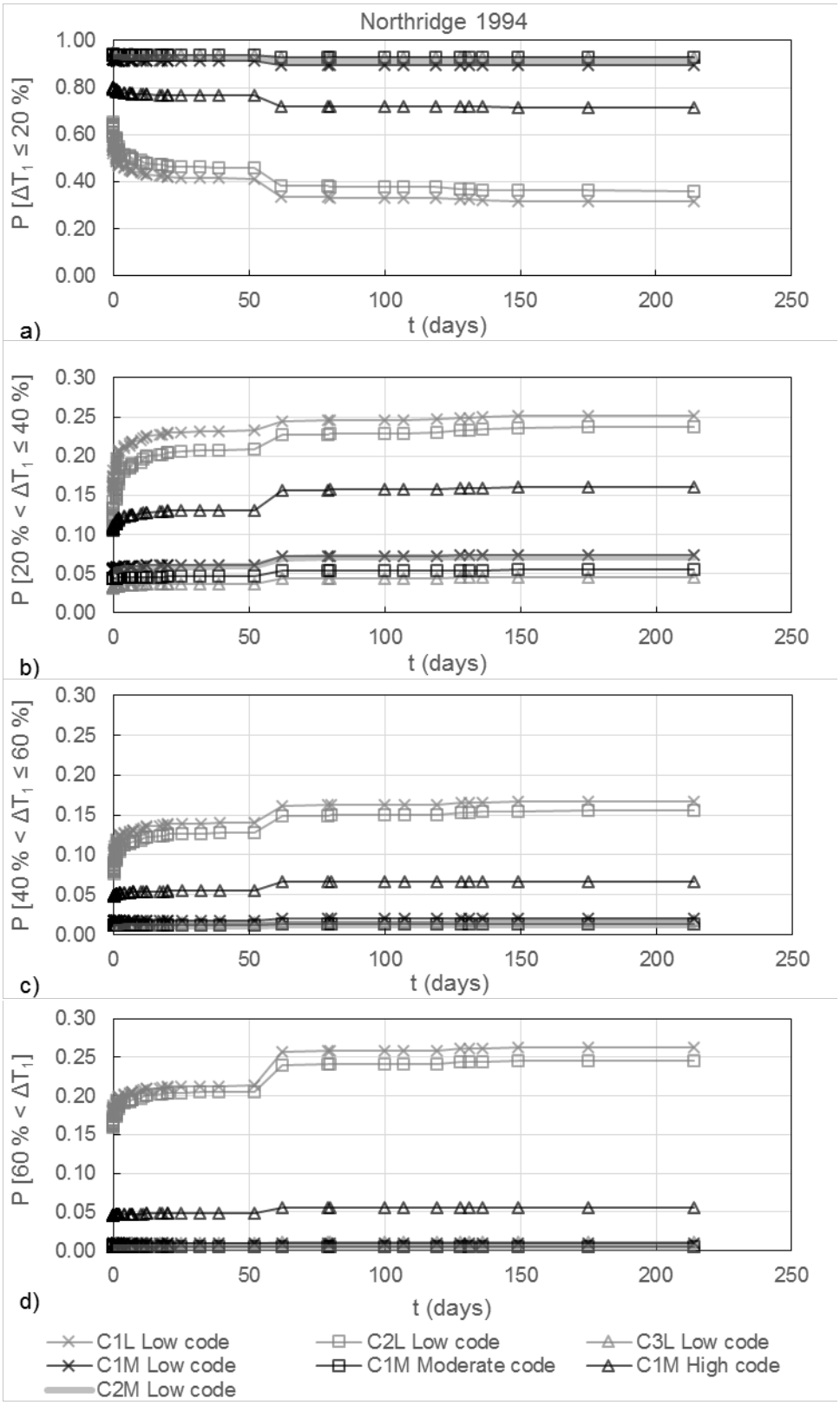

Fig. 12 Probabilities of the considered four damage states (a-d) defined by period elongation (ΔT_1) thresholds of 20 %, 40 % and 60 % in the case of the 1994 Northridge aftershock sequence for the studied building models

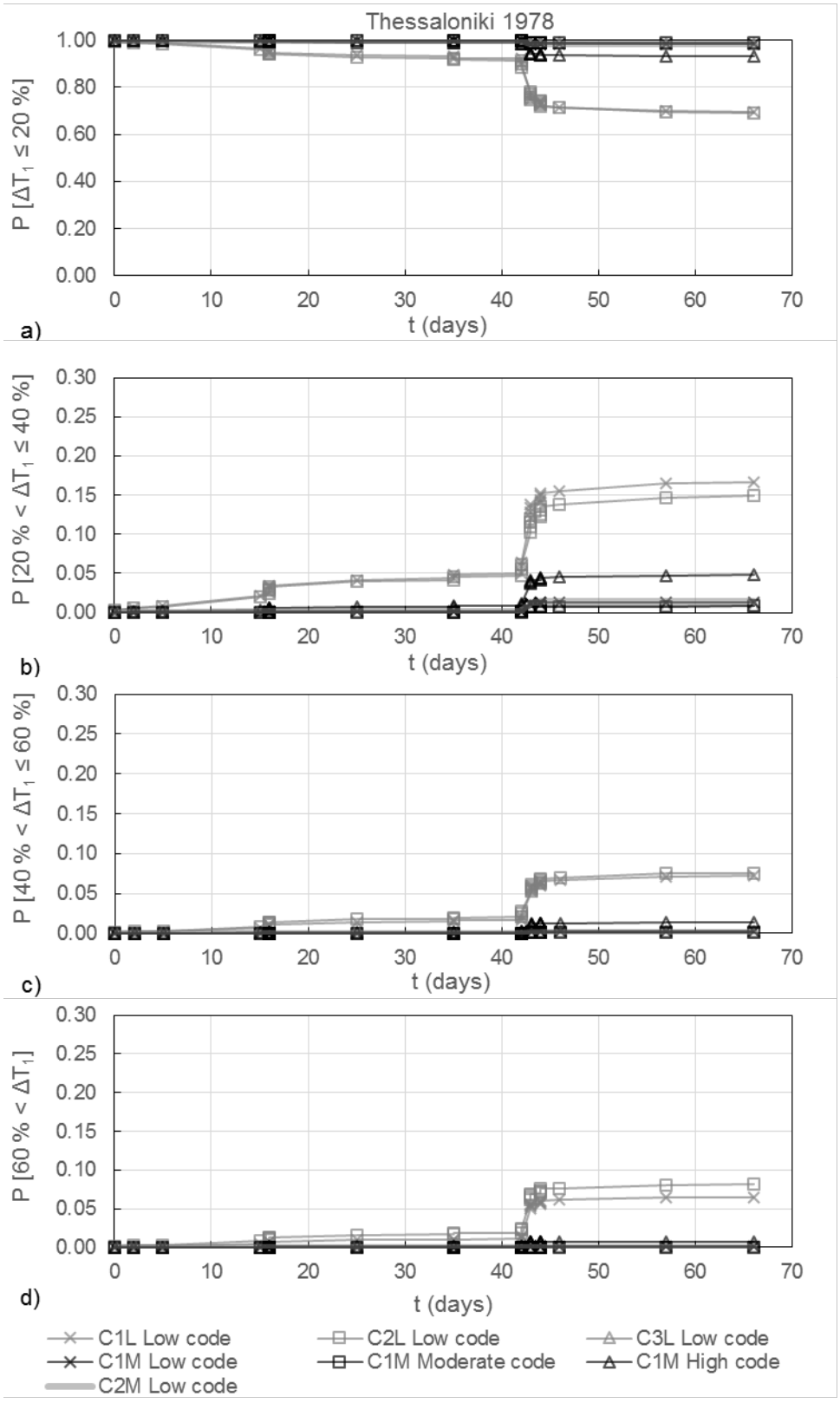

Fig. 13 Probabilities of the considered four damage states (a-d) defined by period elongation (ΔT_1) thresholds of 20 %, 40 % and 60 % in the case of the 1978 Thessaloniki aftershock sequence for the studied building models

According to Zai et al. [54] aftershocks with a PGA less than half the PGA of the main shock can be ignored. In the case of the Northridge sequence all aftershocks –except the aftershock on the 62nd day– have a PGA less than half the PGA of the main shock (Fig. 11b). In Fig. 12 it is observed that aftershocks after the 62nd day do not increase significantly the probabilities of exceeding the damage state thresholds and therefore they could have been ignored. In contrary, the aftershocks before the 62nd day lead to a significant increase of the probabilities to exceed the damage state thresholds. Therefore they should not be ignored, even if their PGAs are less than half the PGA of the mainshock. The significant increase of the probabilities to exceed the ΔT_1 thresholds, which takes place even before the 10th day of the Northridge sequence, is attributed to the high number of aftershocks in that period.

The probabilities of exceedance of the ΔT_1 thresholds are higher for the 1994 Northridge (Fig. 12) than for the 1978 Thessaloniki sequence (Fig. 13) for all models. In both aftershock sequences cases the C1L and C2L low-code and the C1M high-code models exhibit the highest probabilities of exceedance of the ΔT_1 thresholds. The difference between the probabilities of exceedance of the defined thresholds between the C1L and the C3L models is attributed to the presence of infill walls in the C3L model. Additionally, the probabilities of exceedance of the period elongation thresholds for the low-code mid-rise C1M and C2M models are lower than for the low-code low-rise C1L and C2L models. As far as the low-rise and low-period structures are concerned such as the C2L ($T_{1,orig,}$ = 0.18 s) and C3L ($T_{1,orig,}$ = 0.20 s) models, the elongation of their period after the main shock could result to higher spectral acceleration at their first eigenperiod, as spectral values are expected to increase in that range. Therefore, in the case of low-period structures the increase of vulnerability due to structural degradation may be accompanied by the increase of seismic loads.

In Table 7 the probability of exceedance of ΔT_1 equal to 60 % due to the mainshocks and due to all aftershocks in the sequence is listed for the building models in the study. The ratio of these two probabilities for each model and aftershock sequence is also included. This ratio shows the degree to which the threshold of ΔT_1 = 60 % is more probable to be exceeded by the end of the sequences due to damage accumulation and structural degradation than by the main shock. This ratio is higher than 1.0 for all building models and both sequences ranging from 1.19 to 2.07 for the low-rise models and from 1.10 to 1.31 for the mid-rise. A possible explanation of the difference observed between the ratios for the low-rise and the mid-rise models is that the ΔT_1 threshold of 60 % for low-rise models corresponds to less structural damage than for mid-rise models. This is confirmed by the maximum inter-story drifts in Table 3 corresponding to this threshold. The maximum inter-story drift that corresponds to ΔT_1 = 60 % in the case of the C1L and the C1M low-code model is equal to 0.0086 and 0.0137, respectively.

Table 7 Ratio of the probability to exceed a first eigenperiod elongation (ΔT_1) of 60 % due to the aftershock sequences (including the main shocks) to the probability of exceedance only due to the mainshock based on the computation with PGA as the intensity measure

P [ΔT_1 > 60 %]	Thessaloniki 1978			Northridge 1994		
Building Model	Main Shock	Aftershock Sequence	Ratio	Main Shock	Aftershock Sequence	Ratio
C1L Low code	0.03626	0.06464	1.78	0.17760	0.26333	1.48
C2L Low code	0.03950	0.08173	2.07	0.15897	0.24598	1.55
C3L Low code	0.00097	0.00125	1.29	0.00973	0.01160	1.19
C1M Low code	0.00067	0.00077	1.15	0.00893	0.01008	1.13
C1M Mod. code	0.00030	0.00033	1.10	0.00497	0.00546	1.10
C1M High code	0.00541	0.00710	1.31	0.04577	0.05622	1.23
C2M Low code	0.00028	0.00034	1.22	0.00347	0.00414	1.19

Table 8 Probability to exceed period elongation (ΔT_1) of 60 % due to the 1978 Thessaloniki aftershock sequence (including the main shock) according to the computations based on different intensity measures

	P [ΔT_1 > 60%]			
Building Model	PGA	PSA	S_d	$S_{d,m}$
C1L Low code	0.06464	0.01743	0.08219	0.02147
C2L Low code	0.08173	0.06737	0.53248	0.33341
C3L Low code	0.00125	0.00141	0.20930	0.04948
C1M Low code	0.00077	0.00005	0.00016	0.00004
C1M Mod. code	0.00033	0.00001	0.00005	0.00001
C1M High code	0.00710	0.00071	0.00176	0.00060
C2M Low code	0.00034	0.00007	0.00273	0.00021

Table 8 gives the probability of exceedance of ΔT_1 equal to 60 % in the case of the 1978 Thessaloniki aftershock sequence according to the intensity measure. According to the results, the building models, which have the highest and the lowest probability to exceed period elongation of 60 %, regardless of the intensity measure, are the C2L low-code and the C1M moderate-code model, respectively. The probabilities for the low-rise models are generally higher than those for the mid-rise models, especially when S_d and $S_{d,m}$ are considered. Moreover, the computed probabilities in Table 8 for a single building model vary significantly depending on the employed IM. Such differences are anticipated, considering that the probability of exceedance of a damage state threshold for a single seismic event also varies depending on the IM and the dispersion of the fragility curves, and that

differences are increased in a computation for a chain of seismic events as an aftershock sequence.

6. CONCLUSIONS

The elongation of the period of reinforced concrete buildings is considered a reliable and effective measure for assessing probabilistically structural degradation after a strong earthquake. In addition, eigenperiod measurements are considered equally efficient with a red-orange-green traffic light classification based on visual inspection of buildings for signs of physical degradation and can be used complementarily in critical urban areas or buildings part of critical infrastructures. Therefore the presented framework employs the elongation of the first eigenperiod of a building as the engineering demand parameter. Period elongation corresponds to the shift of the period value between before and after an event. It does not correspond to transient period elongation during an earthquake due to inelastic effects. It may not be suitable for structures with significant contribution of higher modes to their response.

The presented framework may be used to assess the variation of the vulnerability of reinforced concrete structures during cascading seismic events and it is applied in the case of two aftershock sequences. The main contribution of this framework is the assessment of vulnerability variation based on period elongation and the potential of the framework to use as input synthetic aftershock sequences. Using as input synthetic aftershock sequences, generated after the mainshock in the context of operational forecasting, offers the potential to assess risk and provide decision-making support in such crisis periods. The proposed procedure can be used for RC buildings with a structural system of moment resisting frames, shear walls, or a dual system and for recorded or forecasted series of seismic events in order to estimate the history of structural deterioration of a building over a time period. Moreover, this framework gives the stiffness degradation ratio of the structural elements of a building and allows a probabilistic localization of seismic damage in RC buildings, which could be used for operative management of a seismic crisis.

A series of results from example applications of the proposed framework for the 1994 Northridge and 1978 aftershock sequences are presented. A comprehensive analysis of seismic risk during aftershock sequences and a sensitivity analysis is out of the scope of this article. According to the results, the vulnerability of reinforced concrete buildings increases due to structural damage accumulation by consequent seismic events. It is shown that the probability of exceeding a damage state threshold due to the main shocks is higher than for any other event in the aftershock sequences of the case studies, but it is only a fraction of

the cumulative probability of exceedance for the duration of the sequences. The probability of damage state threshold exceedance according to the numerical results for the case studies of the aftershock sequences of the 1978 Thessaloniki and the 1994 Northridge earthquake is increasing with time but with a decreasing rate similarly to the increase of the failure probability during an aftershock sequence period as estimated by Iervolino et al. [4]. The probability to exceed ΔT_1 = 60 % during the aftershock sequences is computed equal to 110 % - 207 % of the probability to exceed this threshold due only to the mainshock. It is also observed that the probability of damage increases even for aftershocks with a PGA less than half the predicted PGA for the main shock, although according to other studies the effect of such aftershocks could be ignored [54]. Moreover, the assumption that period elongation of 60 % corresponds to a state near collapse in the case of the mid-rise models is in agreement with the empirical estimations by Katsanos and Sextos [10] of the period elongation of structures with an elastic period of 0.60 s and a force-reduction factor of 3.

In this study, we assume that the response of plane numerical models is representative of the response of the actual three-dimensional buildings, as it is a commonly assumed in seismic vulnerability studies. We also ignore the effect of structural damage accumulation on the damping, and any potential degradation of strength of the structural elements. Furthermore, the sensitivity of the numerical results on the type of input time-histories is not investigated and we assumed a bilinear moment-curvature hysteretic response model for the structural elements acknowledging probable differences in response compared to multi-linear models [55]. In the context of a risk analysis, uncertainties related to PGA and other intensity measures have to be carefully addressed, as well as the sensitivity of structural response on the type of excitation time histories. Moreover a site- and building-specific study, which will account for amplification of ground motion due to site effects, should be conducted in order to obtain realistic risk estimates.

The fact that the framework is based on building period elongation, which is a difference from previous work on this topic, permits to use measurements of building period elongation for updating the starting vector of the Markov chain and thus efficiently updating the assessment of the variation of vulnerability during an aftershock sequence. Therefore, thanks to this framework, we can propose the implementation of an operative Structural Health Monitoring system for building-specific analysis, tracking continuously after a mainshock the variation of frequency and computing the time variation of seismic vulnerability.

AKNOWLEDGEMENTS

The authors thank Prof. Kyriazis Pitilakis of the Aristotle University of Thessaloniki for providing the details of the building models.

The authors also thank Dr. Jacopo Sevla (Istituto Nazionale di Geofisica e Vulcanologia) for suggesting the Markov chain in order to model damage state transitions.

This study was carried out in the framework of the research programme “STREST” – Harmonized approach to stress tests for critical infrastructures against natural hazards (http://www.strest-eu.org) funded by the European Union’s Seventh Framework Programme (FP7/2007-2013, Grant agreement No. 603389).

REFERENCES

[1] Comité Européen de Normalisation. Eurocode 8: Design of structures for earthquake resistance – Part 1: General rules, seismic actions and rules for buildings. EN 1998-1:2004:E

[2] Pitilakis KD, Karapetrou ST, Fotopoulou SD. Consideration of aging and SSI effects on seismic vulnerability assessment of RC buildings. Bulleting of Earthquake Engineering. 2014;12:1777-1803. DOI: 10.1007/s10518-013-9575-8

[3] Sanchez-Silva M, Klutke G-A, Rosowsky DV. Life-cycle performance of structures subject to multiple deterioration mechanism. Structural Safety. 2011;33:206-17. DOI: 10.1016/j.strusafe.2011.03.003

[4] Iervolino I, Giorgio M, Chioccarelli E. Closed-form aftershock reliability of damage-cumulating elastic-perfectly-plastic systems. Earthquake Engineering and Structural Dynamics. 2014;43:613-25. DOI: 10.1002/eqe.2363

[5] Hatzigeorgiou GD, Beskos DE. Inelastic displacement ratios for SDOF structures subjected to repeated earthquakes. Engineering Structures. 2009;31:2744-55. DOI: 10.1016/j.engstruct.2009.07.002

[6] Miranda E, Ruiz-Garcia J. Influence of stiffness degradation on strength demands of structures built on soft soil sites. Engineering Structures 2002;24:1271-81. DOI: 10.1016/S0141-0296(02)00052-4

[7] Mouyiannou A, Penna A, Rota M, Grazziotti, Magenes G. Implications of cumulated seismic damage on the seismic performance of unreinforced masonry buildings. Bulletin of the New Zealand Society for Earthquake Engineering. 2014;47:157-70

[8] Masi A, Vona M. Experimental and numerical evaluation of the fundamental period of undamaged and damaged RC framed buildings. Bulletin of Earthquake Engineering. 2010;8:643-56. DOI: 10.1007/s10518-009-9136-3

[9] Katsanos EI, Sextos AG, Elnashai AS. Prediction of inelastic response periods of buildings based on intensity measures and analytical model parameters. Engineering Structures. 2014;71:161-77. DOI: 10.1016/j.engstruct.2014.04.007

[10] Katsanos EI, Sextos AG. Inelastic spectra to predict period elongation of structures under earthquake loading. Earthquake Engineering and Structural Dynamics. 2015;44:1765-1782. DOI: 10.1002/eqe.2554

[11] Vidal E, Navarro M, Aranda C, Enomoto T. Changes in dynamic characteristics of Lorca RC buildings from pre- and post-earthquake ambient vibration data. Bulletin of Earthquake Engineering. 2014;12:2095-2110. DOI : 10.1007/s10518-013-9489-5

[12] Grünthal G. European Macroseismic Scale 1998. Cahiers du Centre Européen de Géodynamique et de Séismologie;15. Luxemburg: Conseil de L'Europe; 1998

[13] Dunand F, Ait Meziane Y, Guéguen P, Chatelain J-L, Guillier B, Ben Salem R et al. Utilisation du bruit de fond pour l'analyse des dommages des bâtiments de Boumerdes suite au séisme du 21 mai 2003. Mémoires du Service Géologique de l'Algérie. 2004;12:177-91

[14] Jeon J-S, DesRoches R, Lowes LN, Brilakis I. Framework of aftershock fragility assessment-case studies: older California reinforced concrete building frames. Earthquake Engineering and Structural Dynamics. 2015: published online. DOI: 10.1002/eqe.2599

[15] Ebrahimian H, Jalayer F, Asprone D, Lombardi A, Marzocci W, Prota A, Manfredi G. A performance-based framework for adaptive seismic aftershock risk assessment. Earthquake Engineering and Structural Dynamics. 2014;43:2179-2197. DOI: 10.1002/eqe.2444

[16] Yeo GL, Cornell CA. Stochastic Characterization and Decision Bases under Time-Dependent Aftershock Risk in Performance-Based Earthquake Engineering. PEER Report 2005/13. Pacific Earthquake Engineering Research Center: Berkeley CA; 2005

[17] Bindi D, Boxberger T, Orunbaev S, Pilz M, Stankiewicz, Pittore M et al. On-site early-warning system for Bishkek (Kyrgyzstan). Annals of Geophysics. 2015;58:S0112. DOI: 10.4401/ag-6664

[18] Régnier J, Michel C, Bertrand E, Guéguen P. Contribution of ambient vibration recordings (free-field and buildings) for post-seismic analysis: The case of the Mw 7.3 Martinique (French Lesser Antilles) earthquake, November 29, 2007. Soil Dynamics and Earthquake Engineering. 2013;50:162-7. DOI: 10.1016/j.soildyn.2013.03.007

[19] Roux P, Guéguen P, Baillet L, Hamze A. Structural change localization and monitoring through a perturbation-based inverse problem. The Journal of the Acoustical Society of America. 2014;136:2586-97. DOI: 10.1121/1.4897403

[20] Guéguen P, Hamze A, Baillet L, Roux P. Numerical and experimental assessment of the performance of four nondestructive damage evaluation methods in situations comparable to post-earthquake damage analysis. International Journal of Earthquake Engineering. Special Issue: Structural Health Monitoring. 2014;December 01

[21] Kappos AJ, Panagopoulos G, Panagiotopoulos C, Penelis G. A hybrid method for the vulnerability assessment of R/C and URM buildings. Bulletin of Earthquake Engineering. 2006;4:391-419. DOI: 10.1007/s10518-006-9023-0

[22] Federal Emergency Agency. HAZUS-MH 2.1. Department of Homeland Security: Washington DC; 2012

[23] Fardis M, Carvalho E, Elnashai A, Faccioli E, Pinto P, Plumier A. Designer's guide to EN 1998-1 and EN 1998-5 Eurocode 8: Design of structures for earthquake resistance. Thomas Telford Publishing; 2005. DOI: 10.1680/dgte8.33481

[24] Mosalam KM, Günay. Progressive Collapse Analysis of RC Frames with URM Infill Walls Considering In-Plane/Out-of-Plane Interaction. Earthquake Spectra. 2015;31:921-943. DOI: 10.1193/062113EQS165M

[25] EAK 2000 - Greek Antiseismic Code 2000. Earthquake Planning and Protection: Athens; 2001

[26] Penelis GG, Penelis GG. Concrete buildings in seismic regions. CRC Press: London; 2014. DOI: 10.1201/b16399

[27] Kappos AJ, Panagopoulos GK, Sextos AG, Papanikolaou VK and Stylianidis KC. Development of comprehensive earthquake loss scenarios for a Greek and a Turkish city – structural aspects. Earthquakes and Structures. 2010;1:197-214. DOI: 10.12989/eas.2010.1.2.197

[28] Mazzoni S, McKenna F, Scott MH, Fenves GL. Open System for Earthquake Engineering Simulation - user manual. Pacific Earthquake Engineering Research Center: Berkeley CA; 2009

[29] Code for Interventions. Earthquake Planning and Protection: Athens; 2013

[30] Douglas J. Ground-motion prediction equations 1964-2010. PEER Report 2011/102. Pacific Earthquake Engineering Research Center - brgm: Berkeley CA; 2011

[31] Delavaud E, Cotton F, Akkar S, Scherbaum F, Danciu L, Beauval C et al. Toward a ground-motion logic tree for probabilistic seismic hazard assessment in Europe. Journal of Seismology. 2012;16:451-73. DOI: 10.1007/s10950-012-9281-z

[32] Chioccarelli E, Iervolino I. Part 2 (AMRA – Multiple shock capacity reduction for non-evolutionary structural systems). In: Réveillère A, editor. D.4.1 Fragility functions – Impact of repeated events with various intensities on the fragility funtions for a given building typology at local scale. MATRIX – New methodologies for multi-hazard and multi-risk assessment methods for Europe. 2012

[33] Norris JR. Markov chains. Cambridge University Press: Cambridge; 1998

[34] Mackie K., Stojadinovic B. Seismic Demands of Performance-Based Design of Bridges. PEER Report 2003/16. Pacific Earthquake Engineering Research Center: Berkeley CA; 2003

[35] Ambraseys NN, Simpson KA, Bommer JJ. Prediction of horizontal response spectra in Europe. Earthquake Engineering and Structural Dynamics. 1996;25:371-400. DOI: 10.1002/(SICI)1096-9845(199604)25:4<371::AID-EQE550>3.0.CO;2-A

[36] SeismoArtif (Version 2.1) [Computer Program]. Available at: seismosoft.com. Accessed: 30 April 2015. Seismosoft; 2013

[37] Halldorsson B, Papageorgiou AS. Calibration of the Specific Barrier Model to earthquakes of different tectonic regions. Bulletin of the Seismological Society of America. 2005;95:1276-300. DOI: 10.1785/0120040157

[38] Vamvatsikos D. Cornell CA. Incremental dynamic analysis. Earthquake Engineering and Structural Dynamics. 2002;31:491-514. DOI: 10.1002/eqe.141

[39] Zacharenaki A, Fragiadakis M, Assimaki D, Papadrakakis M. Bias assessment in in Incremental Dynamic Analysis due to record scaling. Soil Dynamics and Earthquake Engineering. 2014;67:158-68. DOI: 10.1016/j.soildyn.2014.09.007

[40] Kappos AJ. Seismic vulnerability and loss assessment for buildings in Greece. In: Guéguen P editor. Seismic Vulnerability of Structures. London UK: ISTE Ltd. Hoboken USA: John Wiley & Sons Inc; 2013

[41] Perrault M, Guéguen P, Aldea A, Demetriu S. Using experimental data to reduce the single-building sigma of fragility curves: case study of the BRD tower in Bucharest, Romania. Earthquake Engineering and Engineering Vibration. 2013;12:643-58. DOI: 10.1007/s11803-013-0203-z

[42] Perrault M, Guéguen P. Correlation between Ground Motion And Building Response Using California Earthquake Records. Earthquake Spectra. 2015:31:2027-2046. DOI: 10.1193/062413EQS168M

[43] Luco N, Cornell AC. Structure-Specific Scalar Intensity Measures for Near-Source and Ordinary Earthquake Ground Motions. Earthquake Spectra. 2007:23:357-392. DOI: 10.1193/1.2723158

[44] Papazachos BC, Carydis PG. The time, magnitude and space distributions of the 1978 Thessaloniki seismic sequence. The Thessaloniki, Northern Greece, earthquake of June 20 1978, and its seismic sequence. Technical Chamber of Greece – Section of Central Macedonia; 1983

[45] Hauksson E, Jones LM, Hutton K. The 1994 Northridge earthquake sequence in California: seismological and tectonic aspects. Journal of Geophysical Research. 1995;100:12,335-55. DOI: 10.1029/95JB00865

[46] Thio HK, Kanamori H. Source complexity of the 1994 Northridge earthquake and its relation to aftershock mechanisms. Bulletin of the Seismological Society of America. 1996;86:S84-92

[47] Papazachos BC, Comninakis PE, Karakaisis GF, Karakostas BG, Papaioannou CA, Papazachos CB et al. A catalogue of earthquakes in Greece and surrounding area for the period 550BC-1999. University of Thessaloniki: Thessaloniki; 2000

[48] Papazachos BC, Comninakis PE, Scordilis EM, Karakaisis GF, Papazachos CB. A catalogue of earthquakes in the Mediterranean and surrounding area for the period 1901 – 2010. University of Thessaloniki: Thessaloniki; 2100

[49] Roumelioti Z, Kiratzi A, Benetakos C. The instability of the M_w and M_L comparison for earthquakes in Greece for the period 1969 to 2007. Journal of Seismology. 2009;14:309-37. DOI: 10.1007/s10950-009-9167-x

[50] Papazachos BC, Karakostas VG, Kiratzi AA, Margaris BN, Papazachos CB, Scordilis EM. Uncertainties in the estimation of earthquake magnitudes in Greece. Journal of Seismology. 2002;6:557-70. DOI: 10.1023/A:1021214126748

[51] Akkar S, Bommer JJ. Empirical equations for the prediction of PGA, PGV and spectral accelerations in Europe, the Mediterranean region, and the Middle East. Seismological Research Letters. 2010;81:195-206. DOI: 10.1785/gssrl.81.2.195

[52] Scarlatoudis AA, Papazachos CB, Margaris BN, Theodoulidids N, Papaioannou C, Kalogeras I et al. Empirical peak ground-motion predictive relations for shallow earthquakes in Greece. Bulletin of the Seismological Society of America. 2003;93:2591-2603. DOI: 10.1785/0120030016

[53] Causse M, Laurendeau A, Perrault M, Douglas J, Bonilla LF, Guéguen P. Eurocode 8-compatible synthetic time-series as input to dynamic analysis. Bulletin of Earthquake Engineering. 2014;12:755-68. DOI: 10.1007/s10518-013-9544-2

[54] Zhai C-H, Wen W-P, Li S, Chen Z, Chang Z, Xie L-L. The damage investigation of inelastic SDOF structure under the mainshock-aftershock sequence-type ground motions. Soil Dynamics and Earthquake Engineering. 2014;59:30-41. DOI: 10.1016/j.soildyn.2014.01.003

[55] Dimakopoulou V, Fragiadakis M, Spyrakos C. Influence of modeling parameters on the response of degrading systems to near-field ground motions. Engineering Structures. 2013;53:10-24. DOI: 10.1016/j.engstruct.2013.03.008